Alternative Stress-Resultant Material Modelling in Collapse Analysis of Reinforced Concrete Plates and Shells

Jan A. Øverli
Dr.ing., Research Scientist
SINTEF Civil and Environmental Engineering
N-7456 Trondheim
E-mail: jan.a.overli@civil.sintef.no

Svein I. Sørensen
Dr.ing., Professor
Norwegian University of Science and Technology
Department of Structural Engineering
N-7491 Trondheim
E-mail: svein.sorensen@bygg.ntnu.no

ABSTRACT

This work introduces two material models where the non-linear behaviour of reinforced concrete is defined in terms of stress resultants and generalized strains. The first model utilizes a piece-wise linear moment-curvature curve. In the second material model contributions to the moments and membrane forces are found on basis of the distribution of the principal strains in a cross-section. Compared to analyses employing layered approaches and stress-strain relationships, the stress-resultant material models are superior both with respect to computer time and numerical stability.

Key words: plate, shell, finite element, non-linear analysis, material modelling, stress resultants.

1 INTRODUCTION

Today, non-linear finite element analyses of reinforced concrete structures are commonly used to analyse local problems in a structure. Normally only a small part of the structure is part of a local analysis. In such an analysis the effect of redistribution of forces in the structure is neglected. In some types of structures, like concrete plates and shells, this effect is very important as neglecting it could be both unsafe and uneconomical. The effect of the redistribution of forces would automatically be taken into account if the global finite element model is employed in the non-linear analysis. There are two main reasons why this is not always practicable: computational time and numerical problems. Even with today's computer facilities, a non-linear analysis of a reinforced concrete structure is very time consuming. Normally the analysis is carried out using the layered formulation. Here the cross-section is divided in layers,

and in each layer the response is found on basis of the stress-strain relationship for concrete and reinforcement, see Figure 1(a). An integration through the thickness is then necessary to find the stress-resultants. The numerical problems mainly arise because concrete behaves differently in tension and compression, and is often modelled by different failure criteria. The main objective in this work is to define the material model in terms of stress resultants and generalized strains [1]. Hence, the integration through the thickness to find the stress resultants is avoided. The numerical solution should also be more stable because the response is found on basis of the total cross-section. The stress resultants for a plate or shell are presented in Figure 1(b). The generalized strains are the membrane strains at the middle plane ε, the transverse shear strains γ and the curvatures κ.

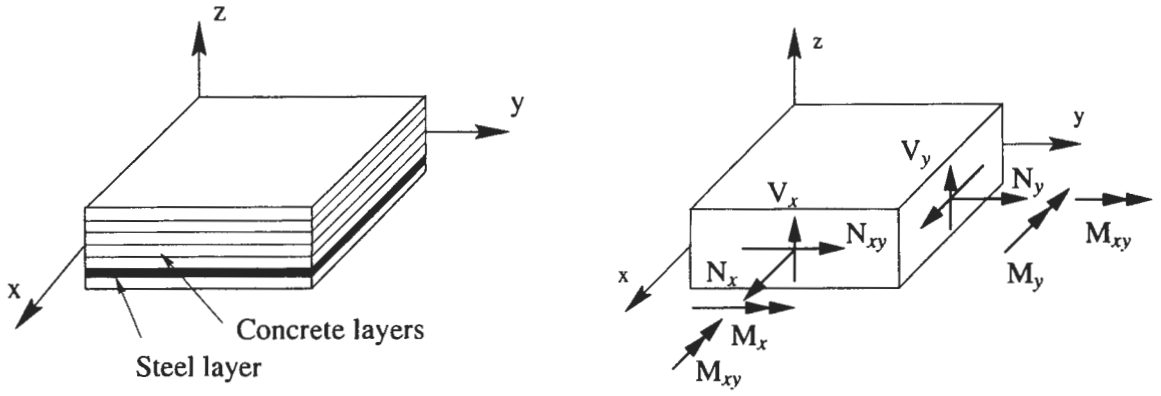

Figure 1 – (a) *Shell divided into layers; (b) Stress resultants acting on a plate or shell element.*

For a general shell the stress resultants and the generalized strains are given as

$$\boldsymbol{\sigma} = \left[N_x, N_y, N_{xy}, V_x, V_y, M_x, M_y, M_{xy}\right]^T$$
$$\boldsymbol{\varepsilon} = \left[\bar{\varepsilon}_x, \bar{\varepsilon}_y, \bar{\gamma}_{xy}, \gamma_{xz}, \gamma_{yz}, \kappa_x, \kappa_y, \kappa_{xy}\right]^T \tag{1}$$

The constitutive relationship is defined as $\boldsymbol{\sigma} = \mathbf{C}\boldsymbol{\varepsilon}$, where $\mathbf{C}$ is the material matrix which for the linear elastic response is given as

$$\mathbf{C} = \begin{bmatrix} \mathbf{C}_N & 0 & 0 \\ 0 & \mathbf{C}_V & 0 \\ 0 & 0 & \mathbf{C}_M \end{bmatrix}, \quad \begin{matrix} \mathbf{C}_N = h\overline{\mathbf{C}} \\ \mathbf{C}_V = G_{\text{eff}} h \mathbf{I}_2 \\ \mathbf{C}_M = \frac{h^3}{12}\overline{\mathbf{C}} \end{matrix}, \quad \overline{\mathbf{C}} = \frac{E}{1-\nu^2}\begin{bmatrix} 1 & \nu & 0 \\ \nu & 1 & 0 \\ 0 & 0 & \frac{1-\nu}{2} \end{bmatrix} \tag{2}$$

Here h is the shell thickness, E is Young's modulus, ν is Poisson's ratio, G_{eff} is the effective shear modulus, $\mathbf{I}_2$ is the identity matrix. For linear elastic response there is no coupling between the membrane, transverse shear and bending deformations.

This paper describes two different stress-resultant material models: (i) a stress-resultant material model for plates without any in-plane forces and (ii) a stress-resultant material model for general shells. The structures under consideration are subjected to short-term static loading. All analyses in this article assume a linear elastic behaviour of concrete in compression and an elastic-perfect plastic behaviour of the reinforcement.

2 STRESS-RESULTANT MATERIAL MODELS

2.1 Resultant plate model

Using constitutive models defined directly in terms of stress resultants is appealing to many engineers as they are used to think in "moments and curvatures". Figure 2(a) illustrates a simplified (piecewise linear) M- curve in the principal moment direction for a reinforced concrete plate, where the principal moments, M_1 and M_2, and the reinforcement, A_{sx} and A_{sy}, do not have the same direction [2]. When a crack is initiated at point A, a distinct change in the stiffness takes place. At point B the reinforcement in one direction starts to yield. At point C the reinforcement in the other direction also yields. What happens beyond point C depends on the amount of reinforcement in the plate. There are also empirical M- relationships, where various assumptions regarding flexural stiffness are employed for different material states [3,4]. It is important to note that when using M- curves, the concrete and the reinforcement are treated as one material.

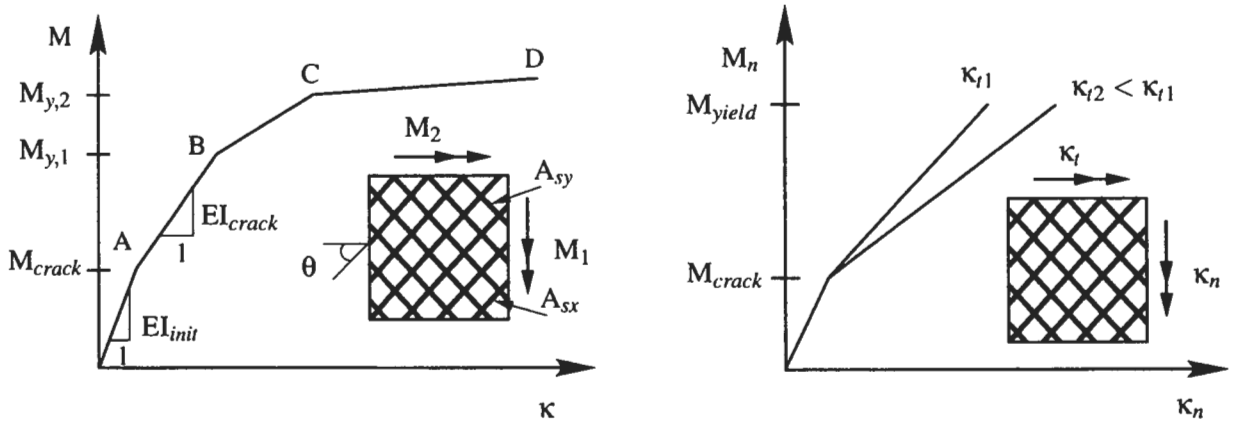

Figure 2 – (a) *Typical moment curvature graph; (b) Dependency of curvature in opposite direction.*

The M- curve presented in Figure 2(a) is only valid for one specific direction. There is a significant effect of the orientation of the reinforcement with respect to the directions of the moments [5]. Even for an isotropic reinforced plate subjected to uniaxial moment, the flexibility can be increased several times as the reinforcement rotates. The M- relationship also depends on the strains perpendicular to the direction under consideration, see Figure 2(b).

The simplified piecewise linear graph in Figure 2(a) is employed as a stress-resultant material model in this work for plate structures without membrane forces. The breaking points on the graph are found by enforcing zero in-plane forces. Thus, this material model is only applicable to concrete plates where the in-plane forces are zero. When finding the breaking points, the tensile stresses in concrete are assumed to be zero. The transverse shear deformations are assumed to be uncoupled from the bending deformations. The linear elastic transverse shear response given in Eq.(2), is assumed to be sufficient in bending dominated problems of plates. A secant unloading path is chosen in the M- relationship.

In the non-linear finite element analyses, cracks are assumed to be in direction of the principal moments, and hence avoiding the definition of the constitutive equations for the twisting moment. An efficient utilization of the stress-resultant plate model requires plate finite elements

without in-plane translational degrees of freedom. However, an iterative procedure is then necessary to find the compression zone heights. The M- r elationship depends both on the angle between the reinforcement and the crack, and on the ratio between the principal moments. Consequently, in an analysis of a two-way slab the relationship needs in general to be recomputed in every equilibrium iteration.

Concrete is not a completely brittle material. Even plain concrete subjected to tensile loading has a post-peak descending branch in a stress deformation diagram. This effect is known as tension softening. In reinforced concrete the concrete block between two adjacent cracks is capable of resisting tensile forces induced because of the bond with the reinforcement. This effect is known as tension stiffening. Tension softening and tension stiffening effects are not directly taken into account when defining M- relationship in the stress-resultant plate model. However, the model does indirectly incorporate some of the effects since it employs a linear curve between the cracking moment and the yielding moment.

2.2 Resultant shell model

Because of the anisotropic nature of reinforced concrete, the principal moments and principal membrane forces do not necessary have the same direction. Compared to a layered model using stress-strain relationships this makes it more difficult to describe a material model when using stress resultants and generalized strains. In addition, the moments and membrane forces are dependent on each other. For steel structures it is possible to use plasticity theory defined in the stress resultant space [8,9]. However, for reinforced concrete this seems like an unattainable task.

In this work a simplified approach is chosen to define the material law by stress resultants. Instead of computing moment-curvature and axial force - membrane strain relationships a more direct method is used. On basis of the strain distribution in a cross-section, compression and tension zones are found and added up to stress resultants. This method has similarities to traditional design of reinforced concrete structures. In contrast to a traditional non-linear layered analysis of shells, the integration through the thickness is avoided. It also avoids the problem having integration points with little stiffness after cracking which often results in numerical problems. This makes the model fast and numerically stable. The model is capable of finding the global response of a reinforced concrete shell structure. The non-linear phenomena of concrete that are taken into account are cracking and yielding of reinforcement.

One of the important and difficult problems in a non-linear analysis of concrete is to define crack directions. When defining the material model in terms of stress resultants, the model has to describe the overall response of the cross-section. Consequently the definition of crack directions is not straightforward. In the finite element formulation the stresses are normally calculated from known strains. In light of this, it is simplest and quickest to employ a strain criterion for cracking. In this work cracks are always assumed to occur in the principal strain directions on the top and/or bottom surface. This is a rotating crack model which has the form of non-linear elasticity. It should be emphasized that the rotation of the crack angle is referred to rotating of principal strains at the faces of the shell. The following assumptions are made regarding cracks in the numerical model:

- Only the in-plane strains are taken into account to find the crack directions.
- The shell is only checked for cracks at the faces.

- The crack direction is constant in the entire tension zone in a cross-section.

By only taking into account in-plane strains when finding the crack directions, only vertical cracks can be formed. Since crack existence is checked only on the surfaces, a maximum of four cracks is possible in the model. Assuming the crack direction is constant in a tension zone can sometimes be a gross error. Having shear membrane strains means the principal strain direction can differ considerably on the face and the beginning of the tension zone. Taken into consideration that the present model is meant to be used in global response analysis of reinforced concrete structures, this should still produce satisfactory results.

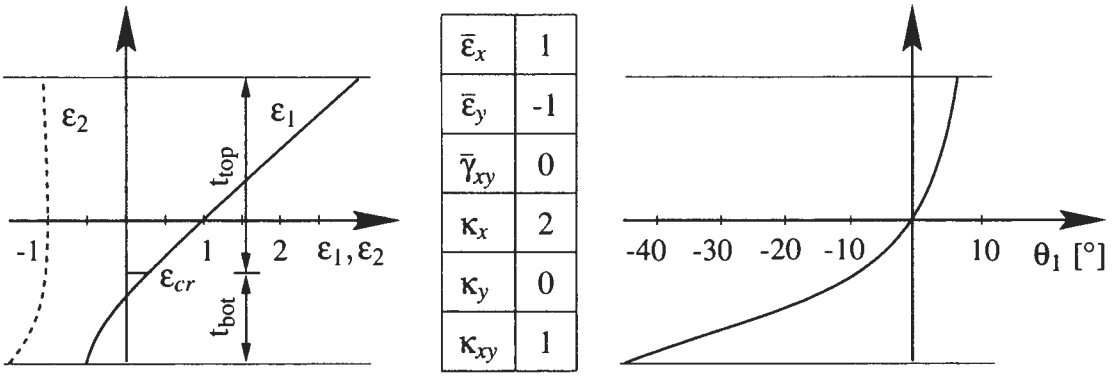

$\bar{\varepsilon}_x$	1
$\bar{\varepsilon}_y$	-1
$\bar{\gamma}_{xy}$	0
κ_x	2
κ_y	0
κ_{xy}	1

Figure 3 - Principal strain distribution in a cross-section with one crack on the top surface.

A general shell has a principal strain distribution over the cross-section which is not linear. Figure 3 presents an example of distribution of principal strains ε_1 and ε_2. The units in the cross-section are chosen so that a curvature of one gives a membrane strain of one at the faces. It must also be noticed that the largest principal strain has different direction on top and bottom faces. On the top face the principal direction is 5° to the ε_x direction, and on bottom it is -45°.

The main idea when finding the stress resultants is to utilize the known principal strain distribution in the cross-section. The cross-section is divided in two parts (layers), t_{top} and t_{bot} in Figure 3. One layer belongs to the top face and the other layer belongs to the bottom face. The border between the two layers are normally defined to be were the largest principal strain equals the concrete cracking strain ε_{cr}, see Figure 3. If this definition does not exist, the border level is defined to be were the maximum principal strain is at the minimum. After dividing the cross-section in two layers, contributions to the sectional forces are calculated separately in each layer. The directions for which this is done are different in the two layers. The calculations are done in the maximum principal strain direction (crack direction) at the actual face. Finally, contributions from reinforcement and concrete are added to the sectional forces.

Figure 4 illustrates a principal strain distribution state which introduces two cracks on the top surface. As seen in Figure 4 the thickness in a layer is not necessary the same in the two principal directions. The resultant concrete force in the lower layer belonging to the direction of largest principal strain is calculated using t^1_{bot}. In direction of smallest principal strain direction, calculation of resultant concrete force is done with t^2_{bot}. Contribution to the shear membrane concrete force is found by employing the smaller of the two thicknesses.

Other possible principal strain distributions can be found in [1].

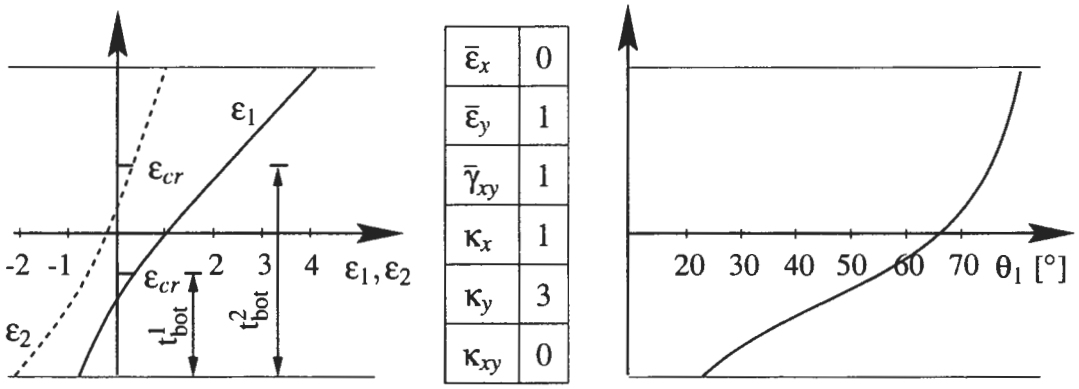

Figure 4 - Principal strain distribution in a cross-section with two cracks on the top surface.

Contributions from tension softening and tension stiffening are added directly to the sectional forces in the stress-resultant shell model. Figure 5 shows the applied curves. The tension softening effect is an isotropic property while additional stresses due to tension stiffening is added in direction of the reinforcement. Parameters in the curves relates to the fracture energy of concrete, crack spacing, tensile strength, a characteristic length to make the strain softening mesh independent, and angle between crack and reinforcement. Detailed description of the applied tension softening and tension stiffening models can be found in [1].

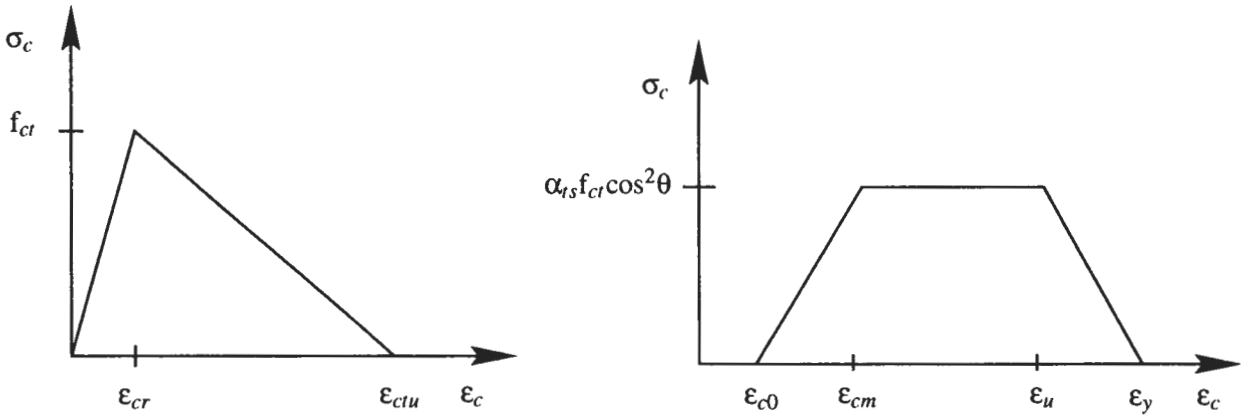

Figure 5 – (a) Tension softening curve; (b) Tension stiffening curve.

2.3 Single element tests

The stress-resultant material models are implemented in the DIANA Finite Element Code [6]. To verify the material models comparison have been made against experimental results. Numerical analyses have been carried out on three slabs tested by Lenschow [5] and Cardenas [7]. The results are also compared to layered finite element analyses. The layered model takes into account the tension stiffening effect by applying a linear descending branch in the tensile stress–strain relationship, with a maximum tensile strain ε_{ctu} = 0.5 ‰, see Figure 5(a). The slabs were loaded by monotonically increasing uniaxial and biaxial moments. The applied moments, definition of reinforcement directions and geometrical and material properties are given in Figure 6.

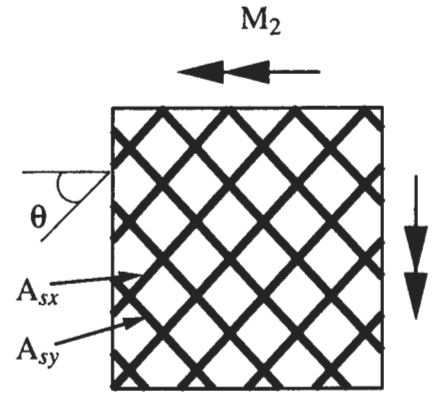

Thickness	h	= 105	mm
Effective height	d	= 89	mm
Concrete compressive strength	f_c	= 35.0	N/mm^2
Concrete tensile strength	f_{ct}	= 3.5	N/mm^2
Young's modulus for concrete	E_c	= 27000	N/mm^2
Young's modulus for steel	E_s	= $2 \cdot 10^5$	N/mm^2
Yield stress for steel	f_{sy}	= 350	N/mm^2

Figure 6 – (a) Applied moments and reinforcement directions in slab element; (b) Geometrical and material properties.

Table 1 provides geometrical data for the slab elements.

Table 1 - Geometrical data for slab elements.

Test	A_{sx} mm^2/mm	A_{sx} mm^2/mm	θ °	M_2 / M_1
B7	0.838	0.914	45	0
B35	0.838	0.914	34	0.45
B39	0.838	0.210	56	0.45

The comparisons of the results obtained in the non-linear analysis and the experimental results are plotted in moment-curvature diagrams in Figure 7-Figure 9. Specimen B7 [5] is loaded with a uniaxial moment. The reinforcement is nearly isotropic and is placed at an angle of 45° to the applied moment. It is seen in Figure 7 that the experimental data obtained and the resultant material models are in close agreement.

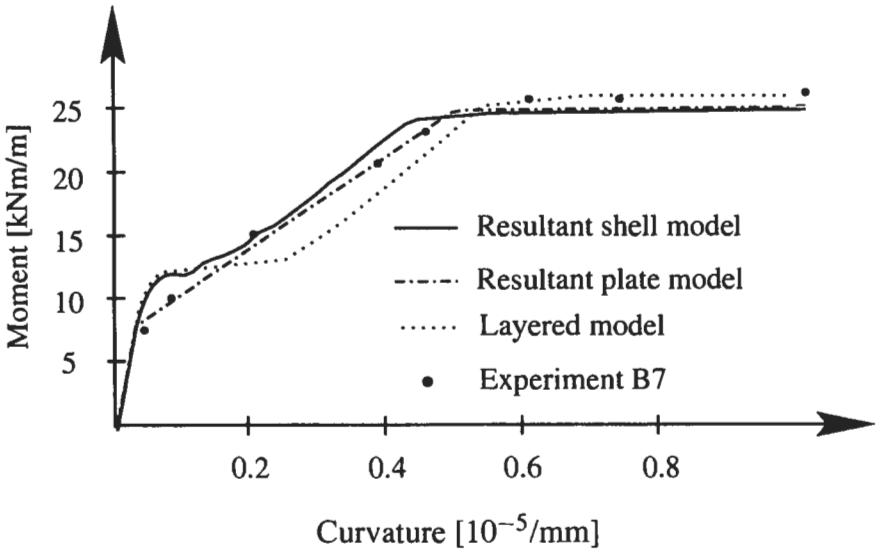

Figure 7 - Slab B7, moment-curvature diagram.

The flexibility and the yielding moment are well predicted. Hence the resultant models are capable of describing the increased flexibility when rotating the reinforcement. Different tension stiffening and tension softening modelling in the material models can explain the difference in results after cracking. The resultant model has more of these effects incorporated. After cracking both the layered and the resultant shell analyses have a bump in the moment-curvature diagram which the experimental results do not have. This is due to the chosen linear tension softening curve. Just after cracking the contribution from tension softening is large. By employing a different curve, for example an exponential curve, the bump effect can be smoothed out. The resultant plate model does not include directly any tension softening and tension stiffening effects. Thus this analysis shows the softest response.

Specimen B35 [7] is loaded with a biaxial moment. The biaxial moment is a combination of a bending and a torsional moment. The reinforcement is still nearly isotropic but is placed at an angle of 34° to the largest applied moment. Figure 8 depicts that the yielding moment obtained experimentally and from the resultant model is nearly equivalent. The yielding curvature is 30% higher for the resultant model than for the experiment. Due to the reinforcement direction of 34°, the cracks rotated up to 5° in the experiment after they were initiated in the applied moment direction. The resultant plate and the layered model were not capable of describing this crack rotation.

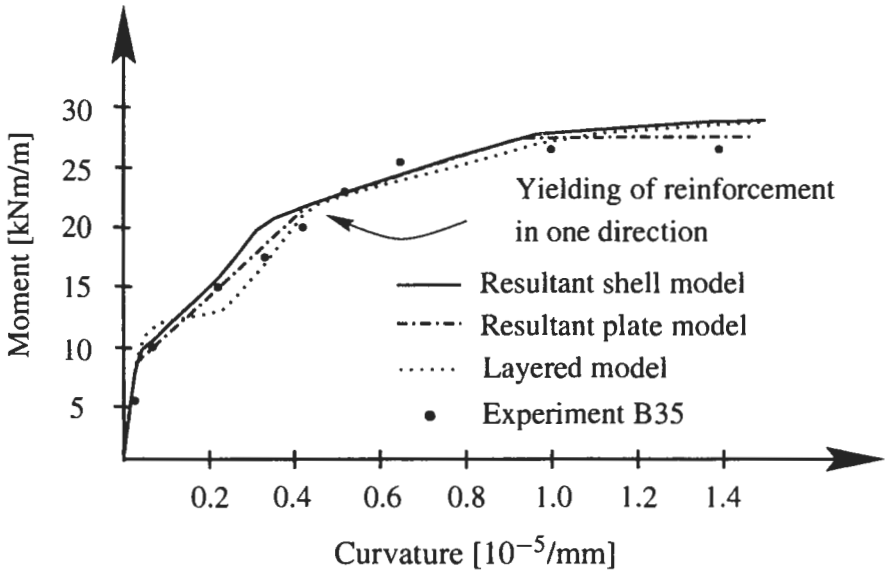

Figure 8 - Slab B35, moment-curvature diagram in the largest moment direction.

The resultant plate model constrains the crack direction to the applied principal moment directions. The layered model utilizes a multiple fixed crack model. The first crack is formed in the applied moment directions. New cracks can form in a multiple fixed crack model if the principal stress exceeds the tensile strength in a direction which is larger than a predefined angle. In these layered analyses this threshold angle is set to 30°. Thus only one crack is formed at each face in this slab. In the analysis employing the resultant shell model the crack initiated by the largest moment rotated 4° before yielding of reinforcement and then rotated back to 0° after yielding. All analyses reached yielding of reinforcement in one direction at a moment level of ~22 kNm/m and produced a clear break in the diagram. However, the experiment did not show any significant change in stiffness at this load level.

Specimen B39 [7] is subjected to a combination of bending and torsional moment. The reinforcement is highly anisotropic and is placed with the strongest reinforcement direction having an angle of 56° to the largest applied moment. As seen in Figure 9 the experiment provides a more flexible response before reaching the yielding moment as compared to the numerical analyses. Due to the anisotropic and skew reinforcement, a large crack rotation takes place in the experiment. The resultant plate and layered model cannot describe this effect because of the constraining of the crack direction. The experimental curve is as expected very difficult to follow between the cracking moment and the yielding moment. With a reinforcement ratio of only 0.2% in one direction, the yielding moment is only 60% higher than the cracking moment. Accurate modelling of tension stiffening and tension softening are henceforth necessary in order to get correlation with the experimental. The yielding moment is well predicted with the resultant models since it is less sensitive to reinforcement orientation and anisotropic reinforcement. Hence the load capacity can still be found in structures with low reinforcement ratios when the failure mode is governed by yielding of reinforcement.

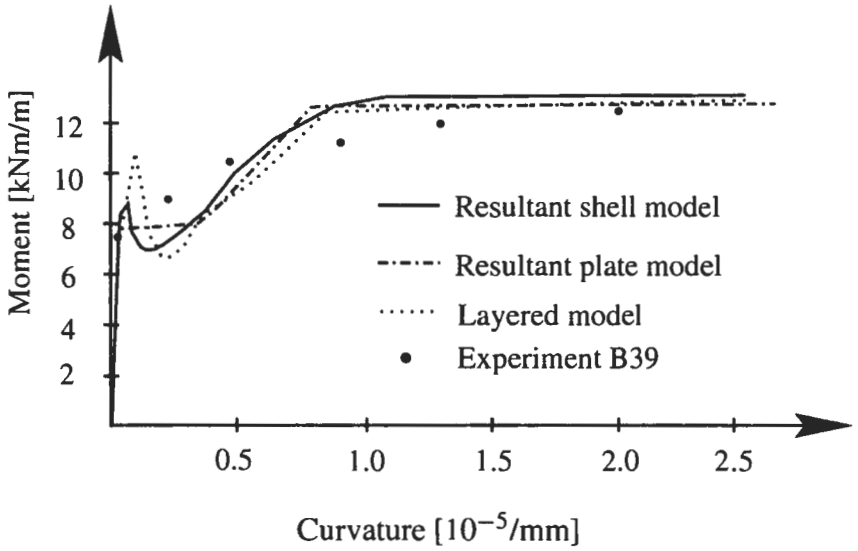

Figure 9 - Slab B39, moment-curvature diagram in the largest moment direction.

The single elements in this section are subjected to pure bending. Analyses with the stress-resultant shell model of elements subjected to both moments and membrane forces have been performed in [1]. The resultant shell model was able to produce results which were in agreement with experiments and analyses using a layered approach.

2.4 *Uniformly loaded square fixed plate*

This example presents an analysis using the stress-resultant material model on a uniformly loaded square fixed reinforced concrete plate. The plate is 10000 mm long and has isotropic reinforcement. A square fixed plate covers most of the non-linearities, which must be considered in a non-linear analysis. Besides the cracking and yielding of the plate also includes cracks inclined to the reinforcement directions. Due to the fixed edge, a redistribution of

moments from the edge to the inner of the plate will take place after the initiation of cracks along the edges. The geometrical and material properties for the plate are

Thickness	$h = 300$	mm
Effective height	$d = 280$	mm
Concrete compressive strength	$f_c = 36.0$	N/mm^2
Concrete tensile strength	$f_{ct} = 3.0$	N/mm^2
Young's modulus for concrete	$E_c = 27000$	N/mm^2
Young's modulus for steel	$E_s = 210000$	N/mm^2
Yield stress for steel	$f_{sy} = 500$	N/mm^2

The reinforcement amounts are constant in the plate and are at both faces and directions 1.0 mm^2/mm. With these low reinforcement ratios the ultimate failure of the plate will be governed by yielding of reinforcement. Geometrical non-linearities are not considered in this work. Therefore it is not possible to describe any increased capacity due to membrane stiffening effects.

The stress-resultant plate model and yield line theory are founded on some of the same assumptions. Hence, a verification of the resultant model is a means of comparing the result to a yield line solution. When having a plate with constant reinforcement ratios, a traditional limit load analysis of a square fixed plate gives a yield load of

$$p_y = 24\frac{M_y + M_y'}{b^2} \tag{3}$$

where M_y is the positive yield moment, M_y' is the negative yield moment, and b is the dimension of the plate. With the reinforcement ratios in this example, the yield moments become 130.2 kNm/m. This produces a yielding load of 62.5 kN/m^2.

To be able to make a direct comparison between the resultant shell model and the layered model, the same tension stiffening model has been applied in these two analyses.

The best way to validate the global response of a structure is to examine the deflections. Figure 10 depicts the deflection at the centrepoint of the plate. As seen, the agreement between the resultant shell and layered models is very good.

The resultant plate model is in good resemblance with the other analyses up to a load level of 40 kN/m^2. After this load level the resultant model reaches its ultimate capacity while in the layered analysis it continues to increase. The difference in capacities can be explained by the enforcing of zero membrane forces in the resultant plate model. After cracking in reinforced concrete the neutral axis will move from the middle plane and introduce horizontal displacements. Due to the different cracking pattern in the middle of the plate and along the edges, the response is a non-uniform in-plane displacement pattern. Even if the plate does not have any horizontal constraints, this introduces membrane forces in the plate. Globally these membrane forces are in equilibrium. The resultant plate model is not capable of describing this because of the absence of in-plane translational degrees of freedom and the assumption of zero in-plane forces. The resultant shell and layered analysis utilizes a general shell element and can therefore describe the non-uniform in-plane displacement pattern. The limit load is also

indicated in Figure 10. Compared to the limit load, the resultant plate analysis predicts the ultimate load carrying capacity with satisfactory accuracy.

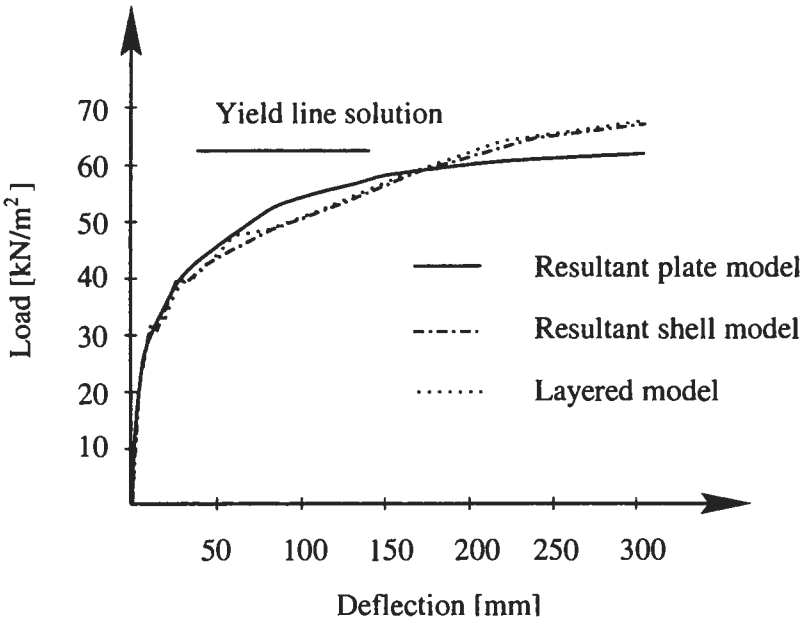

Figure 10 - Load-deflection curve at centre point.

A local validation of the resultant model is to examine the increase in sectional forces. The increase of the maximal moment along the fixed edge, is presented in Figure 11. After cracking, the increase of the moments along the edge starts to decrease. This is due to the redistribution of moments in the plate. A plate with no redistribution (linear elastic analysis) is indicated in the figures. It is seen in Figure 11 that the accordance between the resultant shell and layered analyses is very good. At a load of 20 kN/m^2 the moment at the centrepoint of the fixed edge starts to decrease. An elastic unloading which is assumed in the resultant shell model, is capable of describing this with satisfactory accuracy. At a load of 32 kN/m^2 a global unloading takes place in the plate. This can be seen in both Figure 10 and Figure 11.

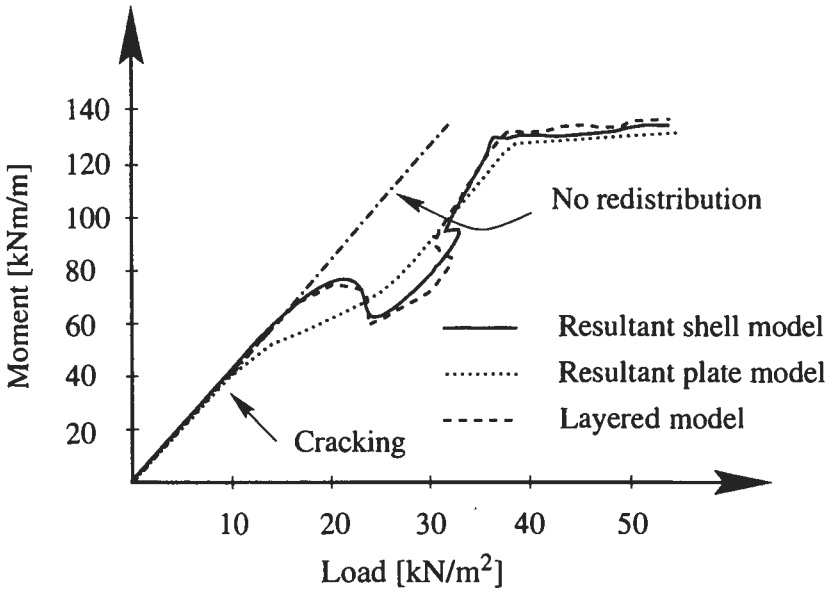

Figure 11 - Moment-load curve at centre point of fixed edge.

Compared to the other analyses the resultant plate model yields too little redistribution. The resultant plate model is also incapable of describing the local unloading which starts at a load of 20 kN/m^2 in the layered and the resultant shell analysis. The yield moment at load level 36 kN/m^2 is well predicted in the resultant model.

3 COMPUTER TIME AND CONVERGENCE

The two main reasons for using a stress-resultant material model are the efficiency and the numerical stability of such a model. Compared to a model using a layered formulation, integration through the thickness is avoided. When looking at the differences in computer time and convergence between the resultant and layered models, the rectangular plate in Section 2.4 was chosen as an example. The layered model had seven integration points through the thickness.

Table 2 presents the CPU-time for one iteration in the plate. These values must not be seen as the absolute differences between the models. The computer time for the layered model varies with the degree of non-linearity such as number of integration points cracked and the chosen number of integration points through the thickness. The computer time for the resultant model is more independent of the degree of non-linearity.

Table 2 - CPU-time for one iteration.

CPU-time [seconds]	Resultant plate model	Resultant shell model	Layered model
Total	1.8	2.6	13.3
Internal force vector	0.7	1.3	10.7

In order to look at the stability of the numerical solution, the number of iterations needed to satisfy equilibrium was counted. In the equilibrium process a regular Newton-Raphson iteration method was used together with an updated normal plane arc-length method. As a convergence criteria a force norm was chosen. Two different tolerances for convergence were tried, 10^{-2} and 10^{-3}. Table 3 specifies the total number of iterations for all load increments needed to satisfy the tolerance for convergence. The analyses were stopped at a load level of 50 kN/m^2. As seen in the table, the resultant based material models need fewer numbers of iterations than the layered model.

Table 3 - Number of iterations up to load level 50 kN/m^2.

Model	Total number of iterations	
	Norm 10^{-2}	Norm 10^{-3}
Layered model	214	579
Resultant plate model	21	53
Resultant shell model	89	188

The total CPU-time and I/O-time up to a specific load level is presented in Table 4. The I/O-time is mainly the time the computer program needs to write and get information from a database. Both resultant models are superior to the layered model.

Table 4 - Total CPU-time up to load level 50 kN/m^2.

Model	CPU-time [seconds]		I/O-time [seconds]	
	Norm 10^{-2}	Norm 10^{-3}	Norm 10^{-2}	Norm 10^{-3}
Layered model	4019	10517	1528	3721
Resultant plate model	38	94	4	7
Resultant shell model	402	784	67	128

The results presented in this section regarding computer time and convergence must not be taken as the absolute differences between stress-resultant material models and analyses employing a layered approach. However, the results do indicate that the resultant material models are computational efficient and numerical stable. Especially the resultant plate model is fast and stable. This can partly be explained by the enforcing of zero in-plane forces when finding the moment- curvature relationship. Hence, unbalanced in-plane forces are not carried over to the global iterative procedure.

4 APPLICATION TO PLATE BRIDGE

4.1 Introduction

The new main airport for Norway opened at Gardermoen outside Oslo in October 1998. In connection with this the motorway out of Oslo has been extended from two to four lanes. New bridges were also built and two bridges had to be removed in connection with this extension. One of the bridges for destruction was Smedstua bridge at Hovinmoen close to Gardermoen. Instead of a regular destruction of the bridge, the Norwegian Roads Administration and the Department of Structural Engineering at the Norwegian University of Science and Technology decided to carry out a full-scale experiment on the bridge. The main idea was to gain more insight and knowledge in the response of large reinforced concrete structures in terms of serviceability and ultimate limit state. Smedstua bridge, which was build in 1989, is a plate bridge with three spans and is symmetrical in a longitudinal direction with respect to the middle of the bridge. It has two driving lanes and one pedestrian lane. The bridge is simply supported at the abutments and has sleeve bearings at the columns and at one of the abutments.

The experimental work was divided in two parts. In serviceability limit state, the bridge was loaded with motor trucks filled with sand. Each truck had a weight of 42.5 tonnes. However, the bridge was heavily reinforced and showed little cracking and small strains when loaded with the trucks. Therefore, this load case will not be further investigated here. In ultimate limit state, a container was built in the middle of the bridge and loaded with sand and gravel. The container was continuously filled with sand and gravel by means of a conveyor belt. To try to achieve an even distribution of the load inside the container a dipping shovel was used. During the loading of sand the deflections and strains in the reinforcement and concrete was measured in the middle and above the columns of the bridge. Both strains in longitudinal and transversal directions were of interest. Figure 12 show shows a picture of Smedstua bridge during the continuously loading

of sand into the container. Detail descriptions of the experimental work and calculations can be found in [10] and [11].

Figure 12 - Smedstua bridge during loading.

4.2 Geometry and material properties

The material characteristics of concrete were found experimentally and are provided in Table 5. After finishing the loading of the bridge examples of the reinforcement were taken to find the average yielding stress.

Table 5 – Experimental found material data

f_c N/mm^2	f_{ct} N/mm^2	E_c N/mm^2	f_{sy} N/mm^2	E_s N/mm^2
48.6	3.8	31100	535	200000

The statical model in longitudinal direction employed in the analyses is illustrated in Figure 13. In transversal direction the bridge is supported in single points at the columns and the abutment. Due to symmetry only half of the bridge is modelled. The middle span is 16.3 m long and the side spans are 11 m long. The non-symmetrical cross-section of the bridge is shown in Figure 14. The thickness of the flanges in the cross-section varies from 200 mm at the outside to 280 mm close to the web. The web of the cross-section has a thickness of 650 mm at the outer and 700 mm at the centre line of the driving lanes. In addition there is a 30 mm concrete wearing surface at the driving lanes. The cross-section is constant in the longitudinal direction of the bridge.

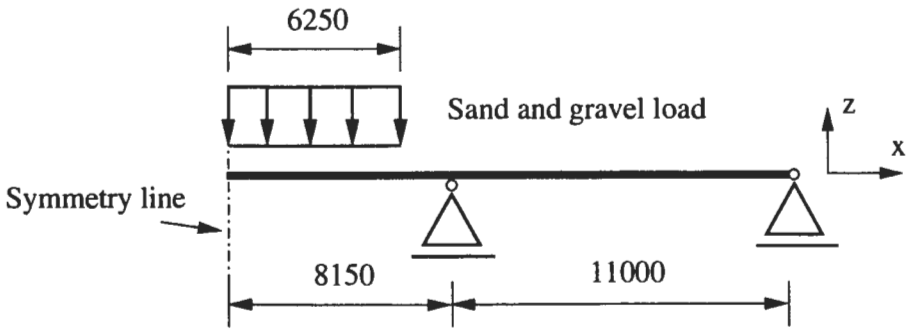

Figure 13 - Statical system with sand and gravel load in middle span.

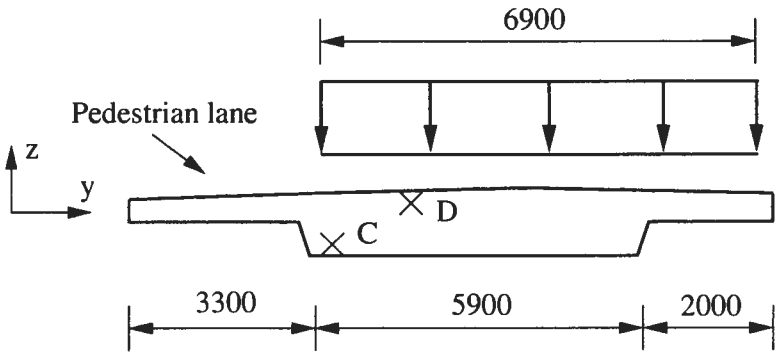

Figure 14 – Cross-section with sand and gravel load in the driving lanes.

Table 6 presents the main reinforcement amounts. In the table, A_{sx} is the reinforcement in longitudinal direction of the bridge. More detailed information about the gradation of reinforcement can be found in [11]. The concrete cover is 45 mm. In addition comes the 30 mm concrete wearing surface. The reinforcement diameter was 25 mm in longitudinal direction and 20 mm in transversal direction of the bridge. Around the columns there is also shear reinforcement. However, shear reinforcement is not part of the stress-resultant material models.

Table 6 – Reinforcement amounts.

Reinforcement	Columns		Middle span		Side Span	
	Flange	Web	Flange	Web	Flange	Web
A_{sx}^{top} [mm^2/mm]	1.0	12.7	1.0	2.1	1.0	2.1
A_{sy}^{top} [mm^2/mm]	1.3	4.6	1.3	1.3	1.3	1.3
A_{sx}^{bot} [mm^2/mm]	1.0	2.1	1.0	6.6	1.0	2.1
A_{sy}^{bot} [mm^2/mm]	1.3	1.3	1.3	1.3	1.3	1.3

4.3 Finite element model

The element mesh employed in the analyses is shown in Figure 15. The figure also gives the load area and the points simulating the support at the columns and the abutment. In the analyses four-node quadrilateral plate and shell elements were used in the stress-resultant plate and shell model respectively. The element model consists of 480 elements and 525 nodes.

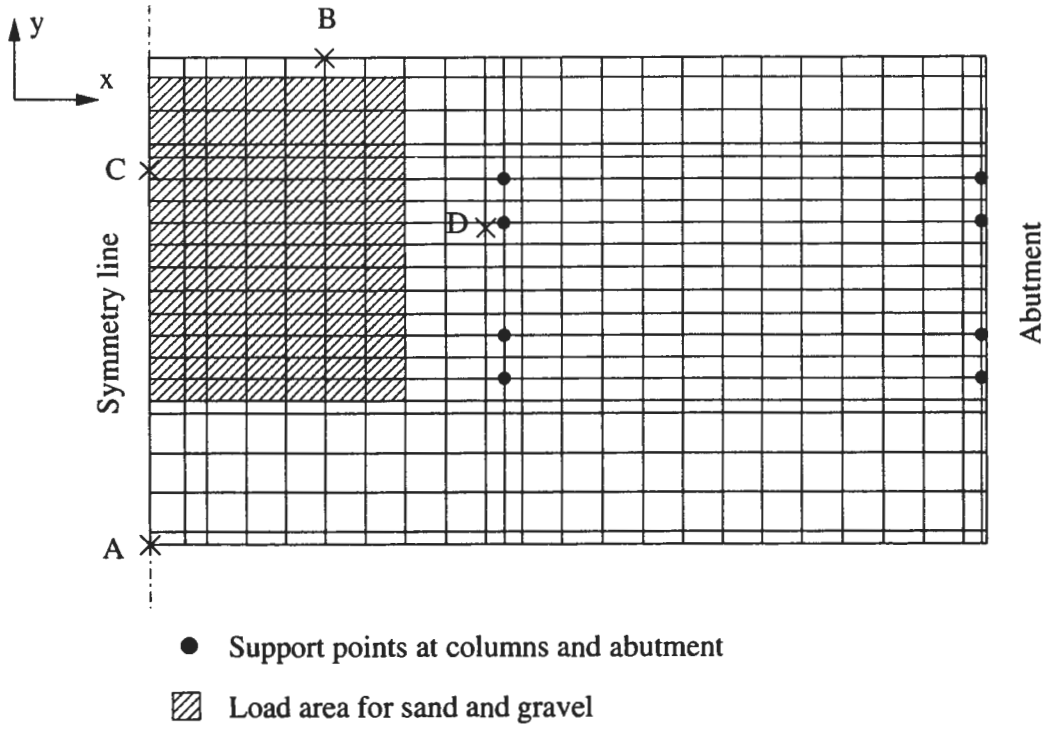

Figure 15 – Element mesh with supports and load area.

4.4 Results

This section presents the result from non-linear analyses carried out on the Smedstua bridge loaded with the container of sand. Both stress-resultant material models presented in this article are employed. The bridge does not have any external membrane forces and the internal membrane forces are small. Hence, the stress-resultant plate model is applicable. The bridge is old which makes it impossible to find the response in the bridge before starting to load the sand and gravel. Thus, when making a comparison of displacements and strains between the experiment and analyses, only the response due to the sand load is considered. The non-linear analyses are divided in two load steps. The first load step is the weight of the bridge itself and the second is the sand and gravel load. No effect of creep and shrinkage of concrete is taken into account.

The container in the middle of the bridge had an area of 6.9 x 12.5 m. The height of the container was 4.5 m. Completely filled with sand and gravel this corresponded to a weight of 830 tonnes. In the transversal direction, the load was placed on the two driving lanes as illustrated in Figure 14. To avoid the bridge rising at the abutments, motor trucks loaded with sand were placed above the supports. Unfortunately, the bridge did not break down with the maximum sand and gravel load of 830 tonnes. According to the Norwegian design code for concrete structures [12] the bridge had a shear capacity around the columns corresponding to a load of 360 tonnes. To initiate a failure mechanism the statical system of the bridge was changed in two steps. First one of the motor trucks placed above the abutments was taken away. The bridge responded with an upward deflection at this abutment of 5-10 cm. Second, the other motor truck was also removed. After a few seconds the bridge collapsed in the middle span. The failure section was in the quarter point of the middle span due to the gradation of the reinforcement. Figure 16 shows a picture of Smedstua bridge after failure load. A simulation of

the change in statical system so as to find the failure load is not performed in these non-linear analyses.

Figure 16 – Smedstua bridge after failure.

In the graphs presenting results from the analyses, only the response due to the sand and gravel load is considered. Figure 17 and Figure 18 depict the load-deflection curves obtained from the experiment and the non-linear analyses. The first graph shows the results in the middle of the bridge at the pavement side, point A in Figure 15. The second graph shows the results in at the quarter point of the middle span at the load side of the bridge, point B in Figure 15. The agreement between the stress-resultant shell model and the layered model, as observed in the figures, is very good. Hence, the different tension stiffening formulations in the two models do not influence the results. In the quarter point of the middle span, point B, the analyses predict the response with satisfactory accuracy compared to the experiment. However, in the middle of the bridge, point A, there is a deviation between the analyses and the experiment. The difference can be explained by two factors:

- Non-uniform distribution of the load.
- Contributions from sand and gravel to the compression zone in the cross-section.

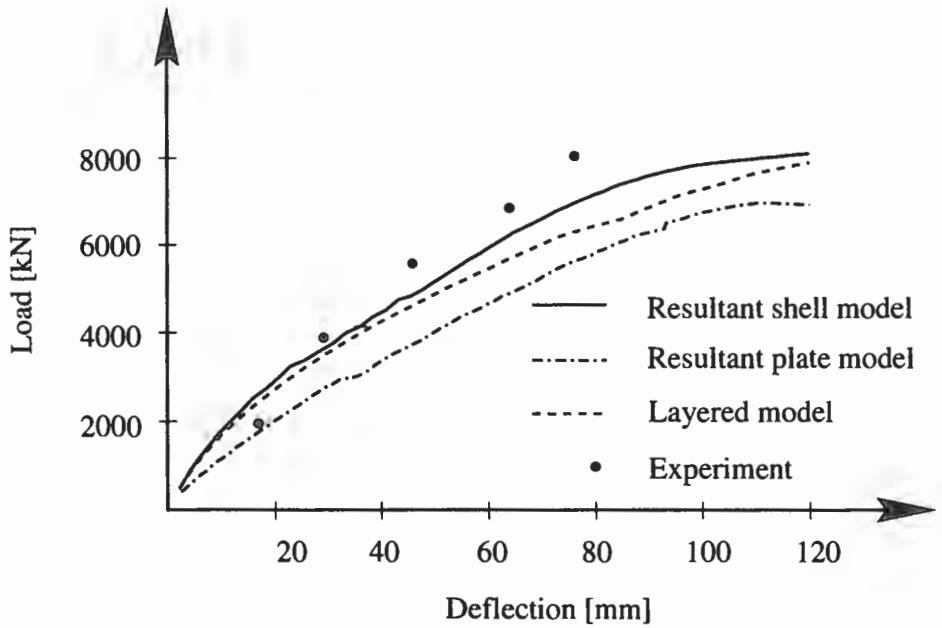

Figure 17 - Load-deflection curve in the middle of the bridge, point A.

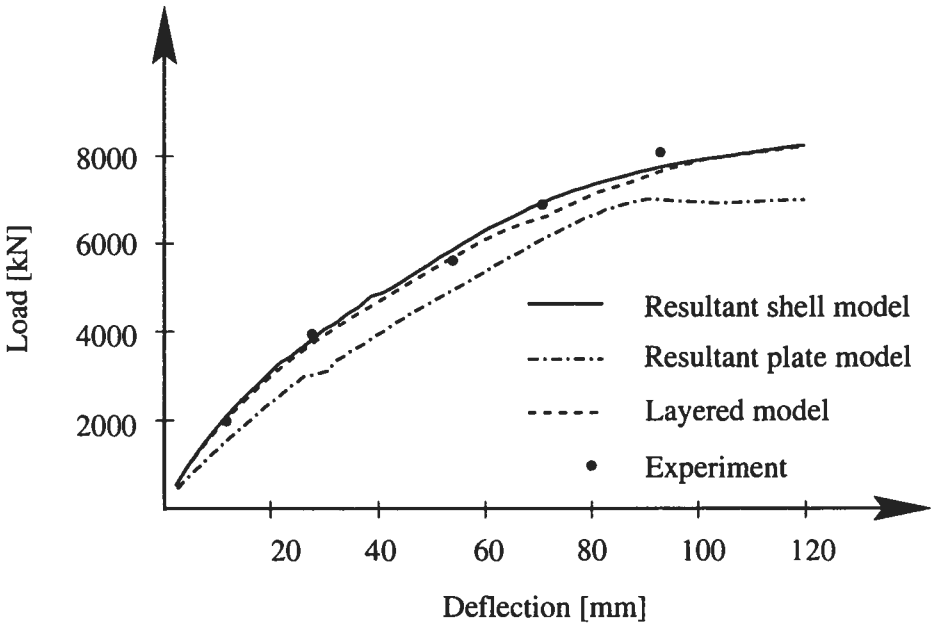

Figure 18 - Load-deflection curve in quarter point of middle span, point B.

The loading container was made by concrete form elements. It was stiffened by placing reinforcement bars in the longitudinal and transversal directions in the entire height. Together with the stiff container the deflection of the bridge introduces an arch effect in the sand and gravel. Consequently, the load is not uniformly distributed as assumed in the analyses. The arch effect also implies contributions from sand and gravel to the effective cross-section. This effect is more pronounced when having the load inside a stiff container. Quantifying these two factors is difficult and is not done here. The factors influence the results more in the middle of the bridge than in areas closer to the columns. The stress-resultant plate model shows a too soft response and too low capacity in Figure 17 and Figure 18. Some membrane forces are introduced in the plate due to the non-symmetrical cross-section and loading area. As for the uniformly loaded square plate in Section 2.4, this can increase the capacity of the structure. The resultant plate model assumes zero in-plane forces and therefore cannot describe this effect. In the plate model the tension stiffening effect is taken into account indirectly and the effect is difficult to quantify. Thus, some of the deviation between the analysis using the plate model and the other two analyses can be explained by the different formulation of the tension stiffening effect.

Figure 19 and Figure 20 depict the strain in the longitudinal reinforcement at the middle and close to the columns of the bridge, points C and D in Figure 14 and Figure 15 respectively. The strains from the resultant and the layered analyses are in close agreement. Experimentally the strains were measured by using strain gauges at the reinforcement bars. As for the load-deflection curves the strains from the analyses produce large deviations compared to the experiment in the middle of the bridge. Some of the deviation can be explained by the arch effect in the sand and gravel. As seen in Figure 17, the deviation starts at a load level of approximately 3500 kN which corresponds to a sand height of 2 m. This is reasonable since a certain height of the sand and deflection of the bridge is needed to build up the arch effect. Close to the columns, the analyses and experiment are in good agreement. The strains in the reinforcement due to weight of the bridge itself are of magnitude 0.1 ‰ in the analyses.

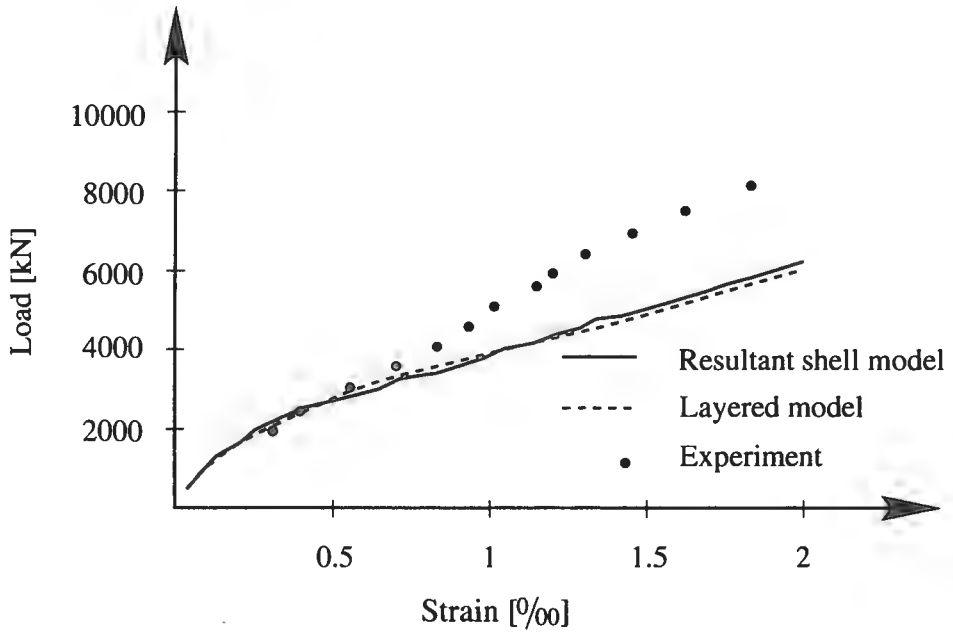

Figure 19 – Strain in reinforcement in the middle of the bridge, point A.

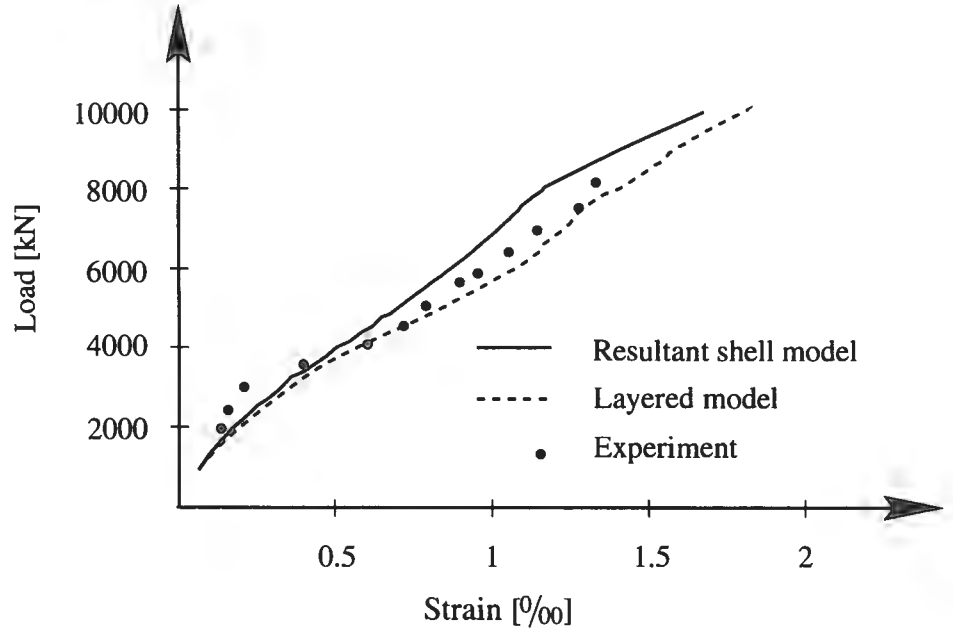

Figure 20 – Strain in reinforcement close to the column, point B.

5 CONCLUSIONS

This work has focused on simplified numerical models for reinforced concrete plates and shells. The constitutive models are defined in terms of stress resultants and generalized strains. This results in computer-efficient models that are capable of describing global non-linear effects such as redistribution of forces in a structure. The limitation of the models is related to problems involving localization, like shear failures, that cannot be properly modelled. The reasons for

employing material models defined with generalized strains and stresses are to save computer time and the numerical stability of such models. Thus, the models are applicable to non-linear analyses of large reinforced concrete structures where these two factors are often critical. In order to verify the stress-resultant material models, comparisons have been made to experimental results and non-linear analyses using a layered approach. The analyses were carried out on both single elements and on larger structures. The resultant material models were capable of simulating the response with satisfactory accuracy. The models were also superior compared to analyses performed using a layered approach as the computer time requirements were greatly reduced.

REFERENCES

1. Øverli, J.A. 1998. *Stress-resultant material models for reinforced concrete plates and shells.* Dr.ing. thesis, Department of Structural Engineering, Norwegian University of Science and Technology, Trondheim, Norway.
2. Frey, F. and Ibrahimbegovi , A. 1993. Stress resultant finite element analysis of reinforced concrete plates. *Engineering Computations,* 10:15-30.
3. Jofriet, J.C. and McNeice, M. 1971. Finite element analysis of reinforced concrete slabs. *ASCE Journal of the Structural Division*, 97(3):785-806.
4. Polak, M.A. 1992. *Nonlinear analysis of reinforced concrete shells.* PhD thesis, Department of Civil Engineering, University of Toronto, Canada.
5. Lenschow, R.J. 1966. *A yield criterion for reinforced concrete under biaxial moments and forces.* PhD thesis, Department of Civil Engineering, University of Illinois, USA.
6. DIANA 1995. *DIANA-Finite element analysis. User's manual release 6.5.* TNO Construction and Building Research, Delft, The Netherlands.
7. Cardenas, A.E. (1968). *Strength and behaviour of isotropically and nonisotropically reinforced concrete slabs subjected to combinations of flexural and torsional moments.* PhD dissertation, Department of Civil Engineering, University of Illinois, USA.
8. Eidsheim, O.M. 1980. *Nonlinear analysis of elastic-plastic shells using hybrid stress finite elements*. Dr.ing. thesis, Division of Structural Engineering, Norwegian Institute of Technology, Trondheim, Norway.
9. Simo, J.C. and Kennedy, J.G. 1992. On a stress resultant geometrically exact shell model. Part V: Nonlinear plasticity: formulation and integration algorithms. *Computer Methods in Applied Mechanics Engineering*, 96:133-171.
10. Langehaug, O., Isaksen, H.R, and Kanstad, T. 1996. Fullskalaforsøk av Smedstua bru (in Norwegian). *Betongindustrien, 28*(3).
11. Rannem Isaksen, H., Kanstad, T., and Olsen, P.-E. 1998. *Prøvebelastning av Smedstua bru, forutsetninger, gjennomføring og måledata* (in Norwegian). Technical Report 98-11 BRU, Public Roads Administration, Directory of Public Roads, Norway.
12. NS3473 1992. *Concrete structure, Design rules*. Norwegian Building Research Institute, NBR, fourth edition.